A coherently stimulated Brillouin spectrometer

Joel N. Johnson,[1, 2, *] Peter T. Rakich,[3] Co Authors,[4] and Ryan O. Behunin[1, 2, †]

[1]*Department of Applied Physics and Materials Science,*
Northern Arizona University, Flagstaff, AZ, 86011, USA
[2]*Center for Materials Interfaces in Research and Applications,*
Northern Arizona University, Flagstaff, AZ, 86011, USA
[3]*Department of Applied Physics, Yale University, New Haven, CT, 06520, USA*
[4]*Department, Address*
(Dated: June 3, 2024)

ALorem ipsum dolor sit amet, consectetur adipiscing elit. Nulla eget dolor at diam volutpat congue sit amet non magna. Phasellus sed ante ornare, commodo elit id, euismod enim. Mauris posuere, erat id vehicula ultrices, erat nisi faucibus lorem, at vehicula enim orci in dui. Nulla facilisi. Integer sed tortor venenatis, aliquet nulla quis, fermentum libero. Proin sit amet metus nec ante fermentum gravida at nec odio. Praesent id nisi ut sapien rutrum hendrerit. Donec vel sapien et eros accumsan tempus. Maecenas non velit nec nulla cursus faucibus sit amet sed dui. Ut eleifend, magna in fermentum efficitur, ligula ipsum blandit libero, sed iaculis eros magna ut arcu. Fusce eget lectus aliquet, consequat dolor at, aliquam urna. Curabitur pharetra, arcu sed vehicula maximus, nibh leo sollicitudin elit, vitae dapibus odio metus gravida ante. Aliquam erat volutpat. Donec venenatis erat vel ultrices suscipit. Nulla consequat massa quis enim. Donec pede justo, fringilla vel, aliquet nec, vulputate eget, arcu. In enim justo, rhoncus ut, imperdiet a, venenatis vitae, justo.

I. INTRODUCTION

Brillouin scattering is the inelastic scattering of light from acoustic phonons. Spontaneous Brillouin scattering is light scattering specifically with the thermodynamic fluctuations in a material. Sufficient optical power elevates this spontaneous process into stimulated Brillouin scattering: a regime in which the optical fields augment the optical properties of the material, greatly enhancing the optomechanical response. This occurs as the backscattered (e.g. Stokes) light beats with the incident pump light to induce an electrostrictive modulation that reinforces the acoustic phonons in the material. It would be desirable to introduce a high-powered fourth optical field dedicated to electrostrictive reinforcement, further stimulating the acoustic field, however phase matching conditions require that its frequency and wavevector be identical to that of the backscattered light, preventing distinguishability.

In this work, we present a coherently stimulated Brillouin spectrometer that utilizes a detuned pump-probe design to perform traveling-wave phonon spectroscopy at scales previously unachievable with traditional stimulated Brillouin techniques. With this method, we achieve sub-10 femtowatt sensitivity and enable room temperature traveling-wave phonon spectroscopy at the micrometer scale. We demonstrate the capabilities of the instrument by observing Brillouin scattering at room temperature in 1 centimeter of UHNA3 fiber and 100 micrometers of bulk carbon disulfide liquid. This instrument opens the door to nanometer-scale Brillouin spectroscopy with

———————

[*] joel.johnson@nau.edu
[†] ryan.behunin@nau.edu

usage of higher optical powers and enables the characterization and development of novel nano-acousto-optic devices.

II. THEORETICAL FRAMEWORK

Coherently stimulated four-wave Brillouin scattering

Stimulated Brillouin scattering, illustrated by the schematic in Fig. 1(a) for the Stokes process, is a three-wave mixing process in which incident pump laser light of frequency ω_{Pump} inelastically scatters from a traveling-wave phonon of frequency Ω to produce light that is frequency-shifted by the phonon frequency. In the Stokes process the phonon is retreating from the incident laser light and the scattered light is shifted down in frequency ($\omega_{Stokes} = \omega_{Pump} - \Omega$). Light scattered in the backwards direction spatially overlaps with the incident laser light, allowing the two optical fields interfere to produce a frequency at the difference between the two ($\omega_{Pump} - \omega_{Stokes}$). Since this difference frequency is exactly equal to the frequency of the acoustic field Ω, the beating of the incident pump light and the backscattered Stokes light produces an electrostrictive reinforcement of the acoustic wave. This driving of the acoustic wave in turn increases the scattering rate of the incident pump light, producing a positive feedback process and an exponential increase of the amplitude of the backscattered Stokes wave.

Fig. 1(b) shows the schematic of coherently stimulated four-wave Brillouin scattering for the Stokes process. We introduce a dedicated external Stokes laser of frequency ω_{Stokes} that strongly drives the electrostrictive reinforcement of the acoustic field in the material. The backscattered Stokes light which is normally collected in

FIG. 1. Illustration of 4-Wave Brillouin Scattering. [stand-in figure]

an SBS process to infer mechanical properties of the material is now drowned out by the much higher power external Stokes laser. To resolve this, we introduce an additional external laser at a distinct frequency ω_{Probe} which copropagates with the pump laser and backscatters in the material from the strongly driven acoustic field. This produces a backscattered signal to be collected ($\omega_{Signal} = \omega_{Probe} - \Omega$) which is distinguishable from the high-powered Stokes laser light.

A full derivation of the coupled-wave equations for this four-wave mixing process can be found in Appendix B, where the scattered power of the backscattered signal is shown to be

$$P_{Signal} = \frac{1}{4}(G_B L)^2 P_{Pump} P_{Stokes} P_{Probe} sinc^2 \left(\frac{\Delta k L}{2} \right),$$

(1)

where G_B is the coherently stimulated Brillouin scattering gain factor,

$$G_B = g_0 \frac{\left(\frac{\Gamma_B}{2} \right)^2}{(\Omega - \Omega_B)^2 + \left(\frac{\Gamma_B}{2} \right)^2},$$

(2)

with the on-resonance gain factor of the material given by

$$g_0 = \left[\frac{\epsilon_0^2 \omega^2 q^4 \gamma_e^4}{n^2 c^2 \rho_0^2} \right].$$

(3)

Here, q is the wavevector of the driven acoustic field, γ_e is the electrostrictive constant, n is the refractive index of the material, ρ_0 is the mean density of the material, Ω_B is the resonant Brillouin frequency of the material, Γ_B is the Brillouin linewidth, or dissipation rate, of the material, and Δk is the wavevector mismatch between the optical fields, to be discussed next.

Phase matching relaxation

In all nonlinear optical processes, efficiency is maximized when phase matching conditions are satisfied. A frequency mismatch (energy unconservation)

or a wavevector mismatch (momentum unconservation) each result in drastically reduced efficiency of a given process.[1] This can be seen by Eq. 1, where the wavevector mismatch, Δk, is contained within a $sinc^2$ function. This $sinc^2$ term thereby defines the phase matching bandwidth of the system, notably scaling with effective interaction length L.

We apply this wavevector mismatch allowance to the pump and probe waves ($\Delta k = k_{Pump} - k_{Probe}$) so that the backscattered signal is different than the applied Stokes wave. This choice allows for selection of the signal and rejection of the Stokes with a bandpass filter. Expressed in terms of wavelengths, this gives

$$\Delta k = \frac{4\pi n \Delta \lambda}{\lambda_{Pump} \lambda_{Probe}} \approx \frac{4\pi n \Delta \lambda}{\lambda_{Pump}^2}.$$

(4)

We can apply this to the phasematching bandwidth term to find the fraction of maximum scattered power, Φ, that can be expected for a given L and phase mismatch $\Delta \lambda$ between the pump and probe,

$$\Phi \equiv sinc^2 \left(\frac{2\pi n \Delta \lambda L}{\lambda_{Pump}^2} \right).$$

(5)

Using this expression for Φ, we see that for an effective length of one meter a wavelength mismatch of only 0.6 pm from 1.55 μm pump light in UHNA3 fiber drops the scattered power to one half of maximum. However, for shorter effective lengths the wavevector mismatch becomes more forgiving; a 36 pm mismatch preserves 82.5% of the maximum signal for a length of 1 cm and all else equal. This separation, translating to about 4.5 GHz, is meaningful, as it represents sufficient spectral separation for the backscattered signal to be isolated from the applied Stokes light.

III. METHODS

Instrument design

The design of the instrument is shown in the schematic in Fig. 2. A pump and Stokes signal is synthesized

FIG. 2. Instrument design diagram

from a single tunable laser source for coherent stimulation of the sample. The pump signal (ω_{Pump}) is amplified by an erbium-doped fiber amplifier (EDFA) and passed through a variable optical attenuator (VOA) for power control. The output is then polarization-controlled to reflect at a polarizing beam splitter (PBS) for injection into the sample. For Stokes synthesis, an AC signal (Ω) is supplied to an intensity modulator with carrier frequency nulled and a tunable filter is used to select one side band output ($\omega_{Pump} - \Omega$). This Stokes light is then amplified by an EDFA, passed through a VOA, and polarization-controlled to reflect at a second PBS for counter-propagation to the pump through the sample.

A separate tunable laser ($\omega_{Probe} = \omega_{Pump} + \Delta k$) is used to synthesize the probe and local oscillator (LO). Probe light is amplified by an EDFA and fed through a VOA. A polarization controller aligns the polarization

axis of the probe light for transmission through the first PBS and copropagation with the pump into the sample. Backscattered probe light exits the sample and transmits back through the first PBS, whereas the orthogonally polarized Stokes light reflects at this same point to be diverted to a tap for power monitoring. The backscattered signal ($\omega_{Signal} = \omega_{Probe} + \Omega$) then routes through two subsequent circulators for spectral filtering by a 5 GHz bandpass tunable filter. This filter allows the frequency-shifted probe light to pass while rejecting (1) any reflected probe light, and (2) any reflected, transmitted, or backscattered pump or Stokes light that was not already diverted by the PBS.

The filtered signal heterodynes via a 99-1 splitter with the LO ($\omega_{LO} = \omega_{Probe} + \omega_{AOM}$), which has been frequency-upshifted 40 MHz by an acousto-optic modulator (AOM) and controlled to be copolarized with the
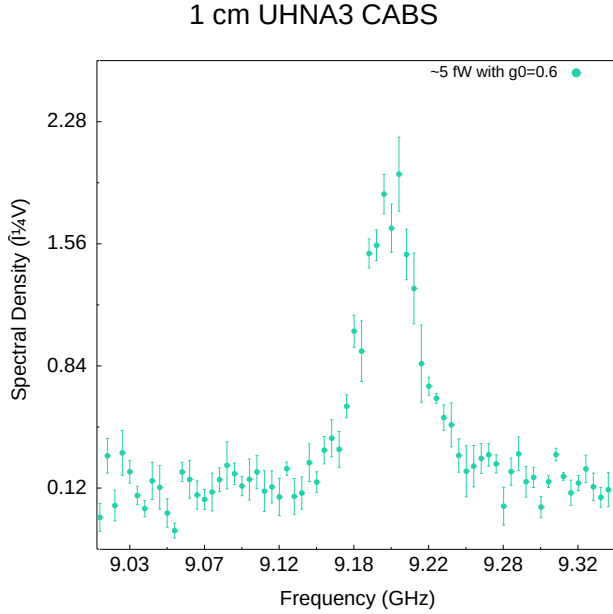
1 cm UHNA3 CABS

FIG. 3. 5 fW sensitivity measurement

backscattered signal. We consider only the subtracted frequency term of the heterodyne process as all others are beyond the range of detection. This heterodyned signal ($\omega_{signal} = \Omega + \omega_{AOM}$) is then captured by a photodiode detector and heterodyned again by a radio frequency (RF) mixer with a second AC signal ($\Omega + \omega_{AOM} - \omega_{Lock}$), where ω_{Lock} is a constant frequency under 50 MHz that the lock-in amplifier is set to read (typically 45 MHz). ω_{Lock} is passed through a 50 MHz low-pass filter, amplified with an RF amplifier, and finally supplied to the lock-in amplifier for data collection. ω_{Lock} remains constant because both AC signals involve Ω and sweep syncronously through the range under measurement.

IV. RESULTS

Instrument sensitivity and SBS comparison

We begin by testing the sensitivity of the instrument as a way of defining a performance metric for the instrument. As well, this figure will serve to inform all future measurements by indicating what material, power, and length combinations might be possible to measure. From Eq. 1, the sensitivity of the instrument is the minimum scattered power, P_{Signal}, to produce a statistically significant measurement. To determine this, we use a sample of known effective Brillouin gain, g_0, and target a specific length, L. We keep the pump-probe detuning, $\Delta\lambda$, constant and record the pump, Stokes, and probe optical powers to calculate the scattered power. Starting with sufficient optical powers to produce a clearly distinguishable measurement, we gradually reduce the optical powers until the sensitivity floor is reached.

We prepared a length of 1 cm of Nufern's UHNA3 fiber to serve as our sensitivity testbed. The properties of UHNA3 fiber are well known and favorable for unambiguous detection of the Brillouin signal. First, it offers a Brillouin shift that is spectrally far from that of the single-mode fiber (SMF28) that constitutes much of our instrument. Additionally, due to its high germanium concentration in the core, UHNA3 fiber has a large refractive index difference between core and cladding, producing exceptionally high optical and acoustic guidance. Finally, UHNA3 fiber offers a high optomechanical nonlinear response; the Brillouin gain of UHNA3 fiber is approximately $0.6\ W^{-1}m^{-1}$ at room temperature[2], which is about an order of magnitude larger than that of SMF28[3].

Fig. 3 shows the Brillouin signal for a sensitivity of $P_{Signal} = [5]\,\text{fW}$. We find the signal-to-noise ratio (SNR) of this measurement to be [>5], determined by taking the ratio of the peak spectral density at the center frequency (9.18 GHz) and the standard error in the spectral density completely off resonance. Assuming a normal noise distrubution profile, an SNR of [5] is equivalent to a $[5]\sigma$ confidence interval, or 99.7% confidence in the statistical significance of this measurement. Parameters for this measurement and calculation of scattered power are listed in Table I.

g_0 $(W^{-1}m^{-1})$	L (m)	P_P (mW)	P_S (mW)	P_{Pr} (mW)	$\Delta\lambda$ (pm)
0.6	0.01	n	m	j	20

TABLE I. Measurement parameters for sensitivity measurement.

The low optical powers required to obtain a measurement of just 1 cm of UHNA3 fiber illustrates the supremacy of the instrument over traditional SBS. An SBS measurement of 1 cm of UHNA3 fiber would require [depends on g0] W of pump power to achieve the same scattered power.

Measurements

We consider two sample types to test the capabilities of the instrument, one fiber-coupled and one bulk material. For a fiber-coupled measurement we again choose UHNA3 fiber for its higher nonlinear response and excellent optical and acoustic guidance. In contrast to the sensitivity measurements, we now apply all available optical power (about 1.5 W) to maximize the backscattered signal from the sample, using the same 1 cm segment of UHNA3 fiber as the target.

Fig. 4 shows the spectral profile captured for 1 cm of UHNA3 fiber, revealing the expected lorentzian profile. The center frequency indicates the Brillouin resonance frequency of the longitudinal mode in the fiber and the FWHM indicates the dissipation rate. The center frequency ([9.18 GHz]) and the FWHM of ([80 MHz]) of
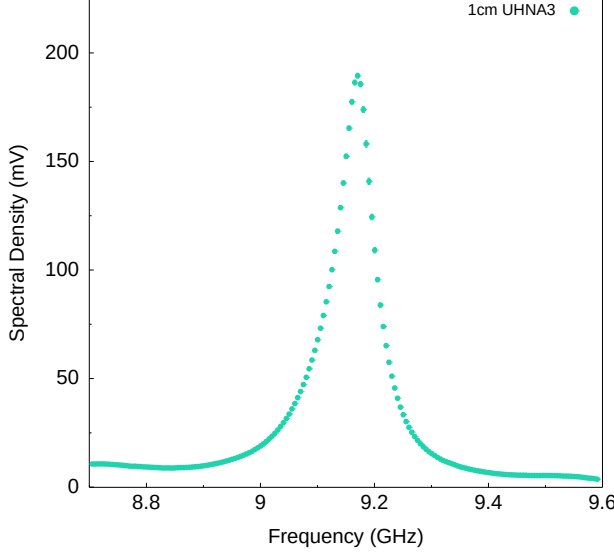
1 cm UHNA3 CABS

FIG. 4. 1cm UHNA3

the measurement match what is seen in the literature.[2] The data shown are an average of five successive measurements and the error bars correspond to 1σ of the standard deviation of the mean, or standard error.
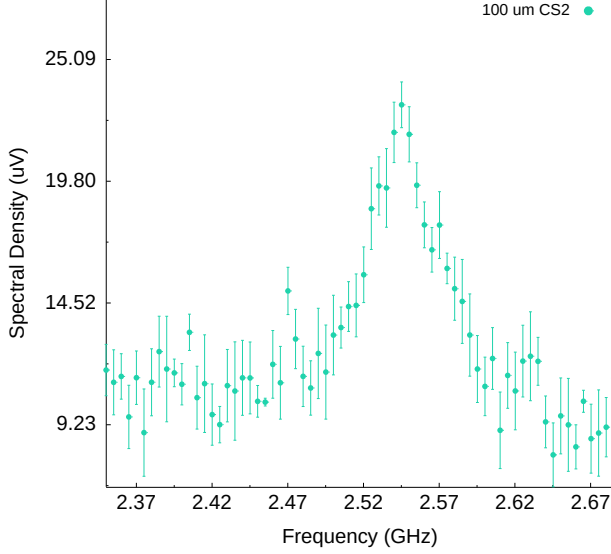
To achieve this measurement of UHNA3 fiber, the instrument design was altered to include only fiber-coupled segments connecting the fiber ports between the two PBSs. The pump laser wavelength was set to 1549.000 nm and the probe laser wavelength was set to 1549.020 nm, giving a frequency mismatch of approximately 2.5 GHz. The pump-probe mismatch is chosen to be only as large as needed to allow the edge of the pass-band of the probe filter to split the backscattered pump and probe light, thus rejecting any backscattered light from the pump laser and accepting only the backscattered signal from the probe laser. The Stokes filter was placed at 1549.073 nm, an offet of approximately 9.18 GHz from the pump laser to capture the Stokes sideband from the intensity modulator. This corresponds to the center of the measured frequency range and was chosen to allow the Stokes sideband output from the intensity modulator to remain within the pass band of the Stokes filter as the RF signal fed to the intensity modulator is swept through the full measurement range. The probe filter was set to 1549.109 nm, an offset of approximately 11.18 GHz from the probe laser, to capture the Stokes-shifted backscattered signal from the probe. The center frequency of the backscattered signal is of course shifted 9.18 GHz from the probe laser, however an extra offset of 2 GHz is chosen for improved rejection of any pump light as the pass band of our filter extends approximately 2.5 GHz on either side of center.

For the UHNA3 measurement shown as well as for all typical measurements, the pump laser emits approx-

imately 45 mW of power, of which 10% is split and amplified to approximately 0.5 W to become the pump optical field. The other 90% emitted from the pump laser is shifted to become the Stokes optical field and is amplified to approximately 1 W. Similarly, the probe laser emits approximately 45 mW of power, of which 10% is split and amplified to approximately 1 W to become the probe optical field and the remaining 90% is used as the LO. To minimize loss to the backscattered signal before being collected by the detector, a 99/1 splitter is used to heterodyne the signal and LO, preserving 99% of the signal power and 1% of the LO power. To compensate for this, The LO is amplified to approximately 230 mW prior to combining with the signal, resulting in the maximum allowable input power for our detector of <2.4 mW incident at the detector. Post-detector, the electronic signal is amplified by a 23 dbm RF amplifier and finally inserted into the lock-in amplifier. For all measurements, it was found that setting both pump and probe lasers to emit in whisper mode (as opposed to dither) dramatically improved the spectral density and SNR of the signal recieved by the lock-in amplifier.

The signal input and demodulator settings of our Zurich Instruments HF2LI 50 MHz lock-in amplifier have been found to be critical for maximizing the SNR of the measurement. First, clock timing is synced between the signal generater and the lock-in with a 10 MHz reference signal output from the signal generator and fed into the lock-in. The range, which defines the gain of the analog input amplifier, should exceed the incoming signal by roughly a factor two including a potential DC offset. This is best chosen by selecting the auto feature within the lock-in software interface, which automatically adjusts the range according to a rolling 100 ms window of the maximum measured input signal amplitude. The coupling mode is set to AC which inserts a high-pass filter that rejects DC components of the input signal. The input impedance is toggled to high, stated as approximately 1MΩ. We set the low-pass filter order to the 8th order, which sets the filter to roll off at the maximum 48 dB/oct. Data collection of the input signal is set to the maximum 1.84 million Sa/s.

We find that the input signal drifts less than 100 Hz after all components of the system reach equilibrium temperature (around 30 minutes). We are thus typically able to set the low pass filter bandwidth to 100 Hz without our signal drifting outside of this range even for long measurements of a few hours. For short measurements of less than 15 minutes this bandwidth can typically be reduced to as little as 40 Hz without risk of the signal drifting out of range. To achieve this precision of the signal input to the lock-in, ω_{Lock}, requires that the frequency difference between the two output signals of the signal generator, $\omega_{Ch1} = \Omega$ and $\omega_{Ch2} = \Omega - \omega_{Lock} + \omega_{AOM}$, be set at least as precisely. While Ω is directly controlled to subhertz precision by the signal generator, ω_{AOM} varies according to the precision of our AOM device. Our AOM has been found to shift its input signal very close to exactly

100 μm CS2 CABS

FIG. 5. 100μm CS2

1 cm UHNA3 Phase-Matching Bandwidth

FIG. 6. Phase-matching sinc func

its specified 40 MHz initially but then gradually increase this shift as the device warms to equilibrium operating temperature over about 35 minutes. At thermal equilibrium, the device is found to shift the signal by approximately 40,000,820 Hz ± 50 Hz. This was found to be the case despite proper thermal grounding of the device.

For a free-space bulk example we target carbon disulfide liquid for its exceptionally high Brillouin gain factor of 1.5 m/GW.[4] Figure 5 reveals the Brillouin signal of carbon disulfide liquid contained in a 100 μm path length cell. To our knowledge, measurement of Brillouin scattering at this scale has not been reported in the literature. A scattered power comparison would reveal that achieving such a measurement using traditional SBS techniques would require excessively high optical powers or cooling the material to cryogenic temperatures, which, of course, would be prohibitive for carbon disulfide in the liquid state.

For this measurement of carbon disulfide, the pump and probe laser wavelengths were set to 1548.808 nm and 1548.898 nm, respectively. The short path length of the sample significantly broadens Φ, the $sinc^2$ term defining the phasematching bandwidth, allowing for further separation of the pump and probe wavelengths for improved signal isolation without significant reduction in scattered power of the signal produced in the carbon disulfide. Specifically, the additional pump-probe wavelength separation of 70 pm employed for this measurement compared to the UHNA3 measurement results in a negligible 0.045% reduction in scattered power. This additional separation contributes meaningfully, however, to improved rejection of pump light by the probe filter and thus higher SNR of the signal.

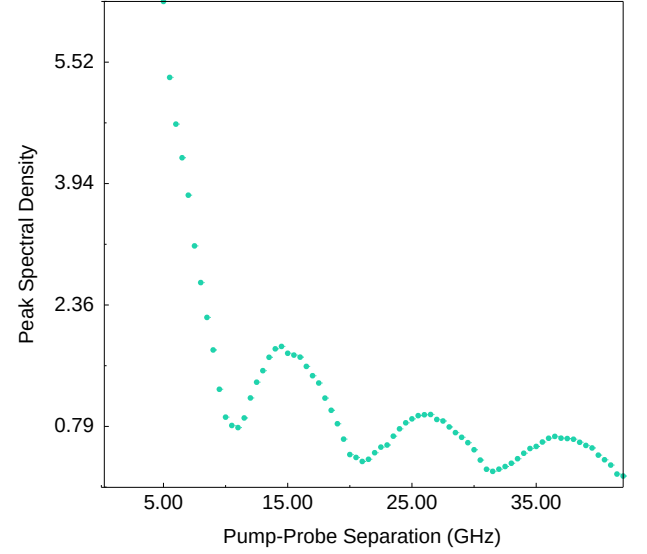Placement of the Stokes filter is critical for measurements of materials that give small Brillouin shifts, such as with carbon disulfide's 2.55 GHz shift. We offset our 5GHz bandwidth Stokes filter an additional 2 GHz to ensure the nearby carrier signal and anti-Stokes sideband from the intensity modulator are rejected and only the Stokes sideband is allowed to pass. For the measurement shown in Fig. 5, this corresponds to a Stokes and probe filter placement of 1548.844 nm and 1548.934 nm, respectively.

V. DISCUSSION

Lorem ipsum dolor sit amet, consectetuer adipiscing elit. Ut purus elit, vestibulum ut, placerat ac, adipiscing vitae, felis. Curabitur dictum gravida mauris. Nam arcu libero, nonummy eget, consectetuer id, vulputate a, magna. Donec vehicula augue eu neque. Pellentesque habitant morbi tristique senectus et netus et malesuada fames ac turpis egestas. Mauris ut leo. Cras viverra metus rhoncus sem. Nulla et lectus vestibulum urna fringilla ultrices. Phasellus eu tellus sit amet tortor gravida placerat. Integer sapien est, iaculis in, pretium quis, viverra ac, nunc. Praesent eget sem vel leo ultrices bibendum. Aenean faucibus. Morbi dolor nulla, malesuada eu, pulvinar at, mollis ac, nulla. Curabitur auctor semper nulla. Donec varius orci eget risus. Duis nibh mi, congue eu, accumsan eleifend, sagittis quis, diam. Duis eget orci sit amet orci dignissim rutrum.

Nam dui ligula, fringilla a, euismod sodales, sollicitudin vel, wisi. Morbi auctor lorem non justo. Nam lacus libero, pretium at, lobortis vitae, ultricies et, tellus. Donec aliquet, tortor sed accumsan bibendum, erat ligula aliquet magna, vitae ornare odio metus a mi. Morbi ac

orci et nisl hendrerit mollis. Suspendisse ut massa. Cras nec ante. Pellentesque a nulla. Cum sociis natoque penatibus et magnis dis parturient montes, nascetur ridiculus mus. Aliquam tincidunt urna. Nulla ullamcorper vestibulum turpis. Pellentesque cursus luctus mauris.

VI.   CONCLUSION

Lorem ipsum dolor sit amet, consectetuer adipiscing elit. Ut purus elit, vestibulum ut, placerat ac, adipiscing vitae, felis. Curabitur dictum gravida mauris. Nam arcu libero, nonummy eget, consectetuer id, vulputate a, magna. Donec vehicula augue eu neque. Pellentesque habitant morbi tristique senectus et netus et malesuada fames ac turpis egestas. Mauris ut leo. Cras viverra metus rhoncus sem. Nulla et lectus vestibulum urna fringilla ultrices. Phasellus eu tellus sit amet tortor gravida placerat. Integer sapien est, iaculis in, pretium quis, viverra ac, nunc. Praesent eget sem vel leo ultrices bibendum. Aenean faucibus. Morbi dolor nulla, malesuada eu, pulvinar at, mollis ac, nulla. Curabitur auctor semper nulla. Donec varius orci eget risus. Duis nibh mi, congue eu, accumsan eleifend, sagittis quis, diam. Duis eget orci sit amet orci dignissim rutrum.

Appendix:

A Coherently Stimulated Brillouin Spectrometer

Appendix B: Coupled-Wave Equations

Here we derive the coupled wave equations that describe coherent stimulated Brillouin scattering involving a pump, Stokes, probe, and backscattered optical field given respectively by

$$\tilde{E}_P(z,t) = A_P e^{i(k_P z - \omega_P t)} + c.c. \tag{B1}$$

$$\tilde{E}_S(z,t) = A_S e^{i(k_S z - \omega_S t)} + c.c. \tag{B2}$$

$$\tilde{E}_{Pr}(z,t) = A_{Pr} e^{i(k_{Pr} z - \omega_{Pr} t)} + c.c. \tag{B3}$$

$$\tilde{E}_{Sig}(z,t) = A_{Sig} e^{i(k_{Sig} z - \omega_{Sig} t)} + c.c. \tag{B4}$$

and a common acoustic field given by

$$\tilde{\rho}(z,t) = \rho_0 + \rho(z,t) e^{i(qz - \Omega t)} + c.c., \tag{B5}$$

where $\Omega = \omega_P - \omega_S$ and $q = k_P - k_S = 2k_P$.

1. Acoustic Field

As in the case of SBS [4], we start by assuming that the material obeys the acoustic wave equation,

$$\frac{\partial^2 \tilde{\rho}}{\partial t^2} - \Gamma' \nabla^2 \frac{\partial \tilde{\rho}}{\partial t} - v^2 \nabla^2 \tilde{\rho} = \nabla \cdot \vec{f}, \tag{B6}$$

where v is the sound speed in the material and Γ' is a damping parameter given by

$$\Gamma' = \frac{1}{\rho} \left[\frac{4}{3} \eta_s + \eta_b + \frac{\kappa}{C_p} (\gamma - 1) \right], \tag{B7}$$

where η_s and η_b are the shear and bulk viscosity coefficients of the material, respectively. The source term on the right side of Eq. (B6) is the divergence of the electrostrictive force:

$$\vec{f} = \nabla p_{st} = \nabla \cdot \left[-\frac{1}{2} \epsilon_0 \gamma_e \left(\langle \tilde{E}_P \cdot \tilde{E}_S \rangle \right. \right.$$
$$\left. \left. + \langle \tilde{E}_{Pr} \cdot \tilde{E}_{Sig} \rangle \right) \right], \tag{B8}$$

which yields, after applying the slowly varying amplitude approximation,

$$\nabla \cdot \vec{f} = \epsilon_0 \gamma_e q^2 (A_P A_S^* + A_{Pr} A_{Sig}^* e^{i\Delta k z}), \tag{B9}$$

Where $\Delta k = (k_{Pr} - k_{Sig}) - (k_P - k_S)$ is the phase mismatch between the four optical fields. Only two electrostrictive terms survive terms after accounting for the orthogonal polarization of the pump and Stokes fields with respect to that of the probe and backscattered signal. Inserting this electrostrictive force term and the acoustic field (Eq. (B5)) into Eq. (B6) and assuming a slowly varying acoustic amplitude we find

$$-2i\Omega \frac{\partial \rho}{\partial t} - \Gamma' 2iq^2 \Omega \rho - 2iqv^2 \frac{\partial \rho}{\partial z} = \epsilon_0 \gamma_e q^2 (A_P A_S^* + A_{Pr} A_{Sig}^* e^{i\Delta k z}), \tag{B10}$$

which can be restated in terms of the Brillouin linewidth, $\Gamma_B = q^2 \Gamma'$, as

$$-2i\Omega \frac{\partial \rho}{\partial t} - 2i\Omega \Gamma_B \rho - 2iqv^2 \frac{\partial \rho}{\partial z} = \epsilon_0 \gamma_e q^2 (A_P A_S^* + A_{Pr} A_{Sig}^* e^{i\Delta k z}). \tag{B11}$$

Given the phonon dispersion relations $\Omega_B = |q_B| v$ and $\Omega^2 = q^2 \left(v^2 - i\Omega \Gamma' \right)$, Eq. (B11) can be rewritten as

$$-2i\Omega \frac{\partial \rho}{\partial t} + \left(\Omega^2 - \Omega^2 - i\Omega \Gamma_B \right) \rho - 2iqv^2 \frac{\partial \rho}{\partial z} = \epsilon_0 \gamma_e q^2 (A_P A_S^* + A_{Pr} A_{Sig}^* e^{i\Delta k z}). \tag{B12}$$

We take the common assumption that the phonon propagation distance is small compared to the distance over which the source term varies significantly, which allows the spatial derivative term in Eq. (B12). We further assume steady-state conditions such that the time derivative term also vanishes, leaving

$$(\Omega_B^2 - \Omega^2 - i\Omega \Gamma_B)_\rho = \epsilon_0 \gamma_e q^2 (A_P A_S^* + A_{Pr} A_{Sig}^* e^{i\Delta k z}). \tag{B13}$$

We thus find the acoustic field amplitude to be

$$\rho(z,t) = \epsilon_0 \gamma_e q^2 \frac{A_P A_S^* + A_{Pr} A_{Sig}^* e^{i\Delta k z}}{\Omega_B^2 - \Omega^2 - i\Omega \Gamma_B}. \tag{B14}$$

2. Optical Fields

We now turn to the spatial evolution of the optical fields, described by the wave equation,

$$\frac{\partial^2 \tilde{E}_i}{\partial z^2} - \frac{n^2}{c^2}\frac{\partial^2 \tilde{E}_i}{\partial t^2} = \frac{1}{\epsilon_0 c^2}\frac{\partial^2 \tilde{P}_i}{\partial t^2}, \tag{B15}$$

where i denotes the four optical fields, namely: pump, Stokes, probe, and backscattered signal. The total nonlinear polarization that gives rise to the source term in the wave equation is given by

$$\tilde{P} = \epsilon_0 \Delta\chi \tilde{E} = \epsilon_0 \Delta\epsilon \tilde{E} = \epsilon_0 \rho^{-1}\gamma_e \tilde{\rho}\tilde{E}. \tag{B16}$$

The parts of $\tilde{P}$ that can act as phase-matched source terms for the optical fields are

$$\tilde{P}_P = p_P e^{i(k_P z - \omega_P t)} + c.c. = \frac{1}{2}\epsilon_0 \rho_0^{-1}\gamma_e \rho A_S e^{i(k_P z - \omega_P t)} \tag{B17}$$

$$\tilde{P}_S = p_S e^{i(-k_S z - \omega_S t)} + c.c. = \frac{1}{2}\epsilon_0 \rho_0^{-1}\gamma_e \rho^* A_P e^{i(-k_S z - \omega_S t)} \tag{B18}$$

$$\tilde{P}_{Pr} = p_{Pr} e^{i(k_{Pr} z - \omega_{Pr} t)} + c.c. = \frac{1}{2}\epsilon_0 \rho_0^{-1}\gamma_e \rho A_{Sig} e^{i(k_{Pr} z - \omega_{Pr} t)} e^{i\Delta k z} \tag{B19}$$

$$\tilde{P}_{Sig} = p_{Sig} e^{i(-k_{Sig} z - \omega_{Sig} t)} + c.c. = \frac{1}{2}\epsilon_0 \rho_0^{-1}\gamma_e \rho^* A_{Pr} e^{i(-k_{Sig} z - \omega_{Sig} t)} e^{-i\Delta k z}. \tag{B20}$$

Inserting the optical fields (Eqs. B1-B4) and phase-matched source terms (Eqs. B17-B20) into Eq. (B15), we obtain

$$\frac{\partial A_P}{\partial z} + \frac{n}{c}\frac{\partial A_P}{\partial t} = \frac{i\omega_P \gamma_e}{2nc\rho_0}\rho A_2 \tag{B21}$$

$$-\frac{\partial A_S}{\partial z} + \frac{n}{c}\frac{\partial A_S}{\partial t} = \frac{i\omega_S \gamma_e}{2nc\rho_0}\rho^* A_P \tag{B22}$$

$$\frac{\partial A_{Pr}}{\partial z} + \frac{n}{c}\frac{\partial A_{Pr}}{\partial t} = \frac{i\omega_{Pr} \gamma_e}{2nc\rho_0}\rho A_{Sig} \tag{B23}$$

$$-\frac{\partial A_{Sig}}{\partial z} + \frac{n}{c}\frac{\partial A_{Sig}}{\partial t} = \frac{i\omega_{Sig} \gamma_e}{2nc\rho_0}\rho^* A_{Pr} \tag{B24}$$

We again assume steady-state conditions, allowing the time derivative term to be dropped. Plugging in the acoustic

field amplitude (Eq. B14), we arrive at the coupled-amplitude wave equations for the optical fields,

$$\frac{\partial A_P}{\partial z} = \frac{i\epsilon_0 \omega_P q^2 \gamma_e^2}{2nc\rho_0} \frac{A_P|A_S|^2 + A_{Pr}A_{Sig}^* A_S e^{i\Delta kz}}{\Omega_B^2 - \Omega^2 - i\Omega\Gamma_B} \tag{B25}$$

$$\frac{\partial A_S}{\partial z} = -\frac{i\epsilon_0 \omega_S q^2 \gamma_e^2}{2nc\rho_0} \frac{|A_P|^2 A_S^* + A_{Pr}A_{Sig}^* A_P e^{-i\Delta kz}}{\Omega_B^2 - \Omega^2 - i\Omega\Gamma_B} \tag{B26}$$

$$\frac{\partial A_{Pr}}{\partial z} = \frac{i\epsilon_0 \omega_{Pr} q^2 \gamma_e^2}{2nc\rho_0} \frac{A_P A_S^* A_{Sig} + A_{Pr}|A_{Sig}|^2 e^{i\Delta kz}}{\Omega_B^2 - \Omega^2 - i\Omega\Gamma_B} \tag{B27}$$

$$\frac{\partial A_{Sig}}{\partial z} = -\frac{i\epsilon_0 \omega_{Sig} q^2 \gamma_e^2}{2nc\rho_0} \frac{A_P A_S^* A_{Pr} + |A_{Pr}|^2 A_{Sig}^* e^{-i\Delta kz}}{\Omega_B^2 - \Omega^2 - i\Omega\Gamma_B} \tag{B28}$$

Integrating Eq. B28 along the effective length gives the amplitudes of each optical field,

$$A_P = \frac{i\epsilon_0 \omega_P q^2 \gamma_e^2}{2nc\rho_0} \frac{A_P|A_S|^2 + A_{Pr}A_{Sig}^* A_S}{\Omega_B^2 - \Omega^2 - i\Omega\Gamma_B} \frac{e^{i\Delta kL} - 1}{i\Delta k}, \tag{B29}$$

$$A_S = -\frac{i\epsilon_0 \omega_S q^2 \gamma_e^2}{2nc\rho_0} \frac{|A_P|^2 A_S^* + A_{Pr}A_{Sig}^* A_P}{\Omega_B^2 - \Omega^2 - i\Omega\Gamma_B} \frac{e^{-i\Delta kL} - 1}{-i\Delta k}, \tag{B30}$$

$$A_{Pr} = \frac{i\epsilon_0 \omega_{Pr} q^2 \gamma_e^2}{2nc\rho_0} \frac{A_P A_S^* A_{Sig} + A_{Pr}|A_{Sig}|^2}{\Omega_B^2 - \Omega^2 - i\Omega\Gamma_B} \frac{e^{i\Delta kL} - 1}{i\Delta k}, \tag{B31}$$

$$A_{Sig} = -\frac{i\epsilon_0 \omega_{Sig} q^2 \gamma_e^2}{2nc\rho_0} \frac{A_P A_S^* A_{Pr} + |A_{Pr}|^2 A_{Sig}^*}{\Omega_B^2 - \Omega^2 - i\Omega\Gamma_B} \frac{e^{-i\Delta kL} - 1}{-i\Delta k}. \tag{B32}$$

The intensity of the backscattered signal is given by the magnitude of the time-averaged Poynting vector, given by

$$I_i = 2n_i \epsilon_0 c |A_i|^2, \qquad i = 1, 2, 3, \tag{B33}$$

which gives

$$I_{Sig} = \frac{\epsilon_0^2 \omega^2 q^4 \gamma_e^4}{4n^2 c^2 \rho_0^2} \frac{|A_P|^2 |A_S|^2 |A_{Pr}|^2}{(\Omega_B - \Omega)^4 - \Omega^2 \Gamma_B^2} \left| \frac{e^{-i\Delta kL} - 1}{-i\Delta k} \right|^2. \tag{B34}$$

Here we have taken the real part and dropped the very small terms containing the signal amplitude. The squared

modulus term containing Δk can be reduced as

$$\left| \frac{e^{-i\Delta kL} - 1}{-i\Delta k} \right|^2 = \frac{(e^{-i\Delta kL} - 1)(e^{i\Delta kL} - 1)}{(\Delta k)^2} = \frac{L^2}{(\Delta kL)^2}\left[2 - 2\left(\frac{e^{i\Delta kL} + e^{-1\Delta kL}}{2} \right) \right]$$

$$= \frac{2L^2(1 - cos\Delta kL)}{(\Delta kL)^2} = \frac{4L^2 sin^2\left(\frac{\Delta kL}{2}\right)}{\left(\Delta kL\right)^2} = \frac{L^2 sin^2\left(\frac{\Delta kL}{2}\right)}{\left(\frac{\Delta kL}{2}\right)^2} = L^2 sinc^2\left(\frac{\Delta kL}{2} \right) \tag{B35}$$

and the optical fields can be written in terms of the intensities to produce the backscattered intensity of the signal:

$$I_{Sig} = \frac{\epsilon_0^2\omega^2 q^4\gamma_e^4}{4n^2c^2\rho_0^2} \frac{I_P I_S I_{Pr}}{(\Omega_B - \Omega)^4 - \Omega^2\Gamma_B^2}L^2 sinc^2\left(\frac{\Delta kL}{2} \right). \tag{B36}$$

Defining the intensities as $I_i = 2n\epsilon_0 cA_i A_i^*$, the backscattered signal intensity is reduced to [see green writing to far right in onenote coupled wave equations of CABS]

To find the power of the backscattered signal, we would integrate this intensity over the effective area. Approximated for fiber as πr^2 where r is the effective mode field diameter, this becomes

$$P_{Sig} = \pi r^2 \frac{\epsilon_0^2\omega^2 q^4\gamma_e^4}{4n^2c^2\rho_0^2} \frac{P_P P_S P_{Pr}}{(\Omega_B - \Omega)^4 - \Omega^2\Gamma_B^2}L^2 sinc^2\left(\frac{\Delta kL}{2} \right). \tag{B37}$$

Appendix C: Instrument Details

1. **List of Salient Components**

2. **Laser Output: Whisper Mode vs. Dither Mode**

3. **Lock-in Settings**

Appendix D: Experimental Techniques

1. **Background Subtraction: Probe Off, Sample In**

2. **Background Subtraction: Probe On, Sample Out**

3. **Polarization Control Limit**

4. **Pump, Stokes, Probe Polarization Optimization**

5. **Local Oscillator Polarization Optimization**

6. **Lock-in Detector Settings**

7. **Detection Bandwidth**

Appendix E: Pump, Stokes, and Probe Contribute Equally

Appendix F: Comparison to SBS

1. **1 Centimeter UHNA3 Scattered Power**

2. **100 Micrometers CS2 Scattered Power**

Appendix G: Measurement Theory

1. **Heterodyne Detection**

2. **Lock-in Detection**

Appendix H: Sensitivity

1. **Sensitivity Measurements**

2. **Current Sensitivity Limitors**

3. **Ultimate Sensitivity Limitor: Shot Noise**

Appendix I: Alternative Configurations

1. **Mirrored Design**

2. **Radial Acoustic Modes**

3. **Shear Acoustic Modes**

4. **Coherent Anti-Stokes Raman Spectrometer**

[1] P. Maker, R. Terhune, M. Nisenoff, and C. Savage, Effects of dispersion and focusing on the production of optical harmonics, Physical review letters **8**, 21 (1962).

[2] R. Behunin, P. Kharel, W. Renninger, H. Shin, F. Carter, E. Kittlaus, and P. Rakich, Long-lived guided phonons in fiber by manipulating two-level systems, arXiv preprint arXiv:1501.04248 (2015).

[3] M. Nikles, L. Thevenaz, and P. A. Robert, Brillouin gain spectrum characterization in single-mode optical fibers, Journal of Lightwave Technology **15**, 1842 (1997).

[4] R. W. Boyd, *Nonlinear Optics* (Academic Press, 2020).